Nuclear Engineering and Technology 54 (2022) 3943–3948

Contents lists available at ScienceDirect

Nuclear Engineering and Technology

journal homepage: www.elsevier.com/locate/net

Technical Note

Preliminary study of artificial intelligence-based fuel-rod pattern analysis of low-quality tomographic image of fuel assembly

Saerom Seong [a], Sehwan Choi [b], Jae Joon Ahn [c], Hyung-joo Choi [a], Yong Hyun Chung [a], Sei Hwan You [d], Yeon Soo Yeom [a], Hyun Joon Choi [d, *], Chul Hee Min [a, **]

[a] Department of Radiation Convergence Engineering, Yonsei University, Republic of Korea
[b] Department of Artificial Intelligence, Hanyang University, Republic of Korea
[c] Division of Data Science, Yonsei University, Republic of Korea
[d] Department of Radiation Oncology, Yonsei University Wonju College of Medicine, Republic of Korea

ARTICLE INFO

Article history:
Received 8 January 2022
Received in revised form
14 April 2022
Accepted 13 May 2022
Available online 20 May 2022

Keywords:
Single-photon emission computed tomography
Monte Carlo
Nuclear fuel assembly
Artificial intelligence
VGG
GoogLeNet
ResNet

ABSTRACT

Single-photon emission computed tomography is one of the reliable pin-by-pin verification techniques for spent-fuel assemblies. One of the challenges with this technique is to increase the total fuel assembly verification speed while maintaining high verification accuracy. The aim of the present study, therefore, was to develop an artificial intelligence (AI) algorithm-based tomographic image analysis technique for partial-defect verification of fuel assemblies. With the Monte Carlo (MC) simulation technique, a tomographic image dataset consisting of 511 fuel-rod patterns of a 3 × 3 fuel assembly was generated, and with these images, the VGG16, GoogLeNet, and ResNet models were trained. According to an evaluation of these models for different training dataset sizes, the ResNet model showed 100% pattern estimation accuracy. And, based on the different tomographic image qualities, all of the models showed almost 100% pattern estimation accuracy, even for low-quality images with unrecognizable fuel patterns. This study verified that an AI model can be effectively employed for accurate and fast partial-defect verification of fuel assemblies.

1. Introduction

The International Atomic Energy Agency (IAEA) has been developed single-photon emission computed tomography (SPECT) for a reliable pin-by-pin spent-fuel assembly verification owing to its intuitive imaging capability [1–3]. Unlike the conventional volume-averaging method for measurement of spent-fuel assembly radioactivity, SPECT can verify partial defects by acquiring a tomographic image of the assembly and analyzing the radioactivity distribution of the fuel rods therein [4–9]. The IAEA set a goal time for the measurement per assembly with the prototype SPECT system, named Passive Gamma Emission Tomography (PGET), as less than 10 min in 2006 for the fuel with a minimum burn-up of 15 GWd/t and a cooling time up to 40 years [4,5]. On the other hand, Miller et al. [9] reported that the total assay times for the pin-by-pin spent-fuel assembly verification, consistent with IAEA's concept of operations in 2017, were approximately 1–2 h. Nevertheless, still, there are limitations to achieving this time goal with the conventional SPECT system [9], due to various measurement conditions affecting tomographic image quality such as different cooling times and characteristics of fuel assembly geometry.

Our previous Monte Carlo (MC) study [10] showed that clearly acquiring a tomographic image for the ^{137}Cs nuclide emitting 662 keV gamma-rays is difficult in water storage, due to the high probability of attenuation and scattering by water and the high-Z materials of fuel rods. Furthermore, if the scanning speed of the SPECT technique for fuel assembly verification is increased to achieve the IAEA's inspection time goal, the overall amount of measurement data will be reduced, leading to image distortion. Recently, artificial intelligence (AI)-based image processing and analysis techniques have been actively investigated and verified for accuracy [11]. They can help to overcome the above-noted limitations, specifically by learning the correlations between the characteristics of image acquisition under specific conditions and the

* Corresponding author.
** Corresponding author.
E-mail addresses: hjchoi1@yonsei.ac.kr (H.J. Choi), chmin@yonsei.ac.kr (C.H. Min).

https://doi.org/10.1016/j.net.2022.05.013

resulting image. The aim of this study, therefore, was to develop a tomographic image analysis technique for partial-defect verification in a fuel assembly, as based on AI algorithms well known in the visual recognition research area.

2. Materials and methods

2.1. Tomographic image dataset of fuel assembly

MC simulation enables statistical radiation transport analysis using random numbers. With its realistic estimation of specific physical phenomena, it can be an alternative to experimentation performed with high-cost equipment. Using GATE (v. 8.1) MC simulation program [10], we modeled a rotational SPECT system consisting of four 64-channel detectors and used it to obtain projection data for a test fuel assembly (Fig. 1). Each detector consisted of 64 trapezoidal-shaped 3 × 40× 40 (front side) and 3 (back side) mm^3 BGO scintillators along with a tungsten collimator with 64 2 × 50× 40 mm^3 slits. The distance between the detector surface and the fuel assembly center was 220 mm. The fuel assembly was comprised of 3 × 3 fuel-rod arrays positioned at 12.69 mm intervals, the fuel-rod diameter being 9.94 mm. Based on the energy spectrum data reported by Pacific Northwest National Laboratory in 2016 [8], we determined the characteristics of the gamma-rays emitting from each fuel rod by assuming the spent-fuel burn-up and cooling times to be 10327 MWd/MTU and 5 years, respectively. In this assembly condition, the relative atom densities of ^{134}Cs, ^{137}Cs, and ^{154}Eu, emitting 604.7–1274.4 keV gamma-rays, were 5.1%, 100%, and 0.8%, respectively [8]. The predominant energy of the gamma-rays was 662 keV, because the major radionuclide of the spent fuel was ^{137}Cs, owing to its long half-life (about 30 years). A total of 511 tomographic images were acquired for 2^9-1 patterns of missing fuel rods in the 3 × 3 fuel assembly, under the assumption that all fuel rods have the same radioactivity. The fuel rods consisted of UO_2 (10.519 g/cm^3), ZIRLO (6.578 g/cm^3), and He gas (2.222 mg/cm^3). For a 17 × 17 fuel assembly, the number of patterns of missing fuel rods is 2^{289}-1, and there are currently limitations on obtaining MC simulation data for such a large number of patterns. Therefore, in this study, we employed the 3 × 3 fuel assembly for proof-of-principle purposes. Each image was reconstructed within a 64× 64-pixel dimensions by a filtered back-projection (FBP) algorithm, using 400 projection datasets obtained in 0.9° increments during 360° of rotation (i.e. sinogram).

2.2. Determination of AI models

In this study, VGG16, GoogLeNet, and ResNet models were selected from among various AI models that have been developed to deliver higher image classification accuracy with lower power consumption over the past decade. VGG16 and GoogLeNet are deep learning models proposed by Oxford University's Visual Geometry Group (VGG) and Google, respectively, in 2014. These models showed that a deeper-layer structure offers advantages in terms of the image recognition performance of the deep learning model [12] when compared with previous high-performance models consisting of eight layers such as AlexNet [13]. Unlike other types of convolutional neural networks (CNN) that use filters of various local receptive fields, VGG16 simply uses filters of 3 × 3 local receptive fields in all convolution layers. Its advantage is its capacity to not only reduce the number of parameters in the training process but also improve model performance through its deep hierarchical structure, specifically by extracting more nonlinear features as the number of convolution operations increases [14]. GoogLeNet consists of 22 layers and requires 5 million parameters during operation [15]: 2.75-times deeper layers and about 0.08-times smaller parameters than those of AlexNet [13]. GoogLeNet's computational efficiency, moreover, is higher than that of AlexNet, thanks to its inception module that efficiently extracts various features through a parallel (not in-series) connection of convolution operations. In fact, GoogLeNet has nine inception modules using filters of 1 × 1, 3 × 3, and 5 × 5 local receptive fields. In order to solve the gradient vanishing problem in which the gradient gradually converges to zero in the process of backpropagation, GoogLeNet is equipped with auxiliary classifiers in the middle of its hierarchical structure [15–17]. These auxiliary classifiers are used only for model training and are removed after training is completed. When the auxiliary classifiers are applied to training, the slope of the weight change tends to vary according to the number of iterative operations in the training process, resulting in more stable learning outcomes. The ResNet model, structured based on VGG19, is a deep learning model

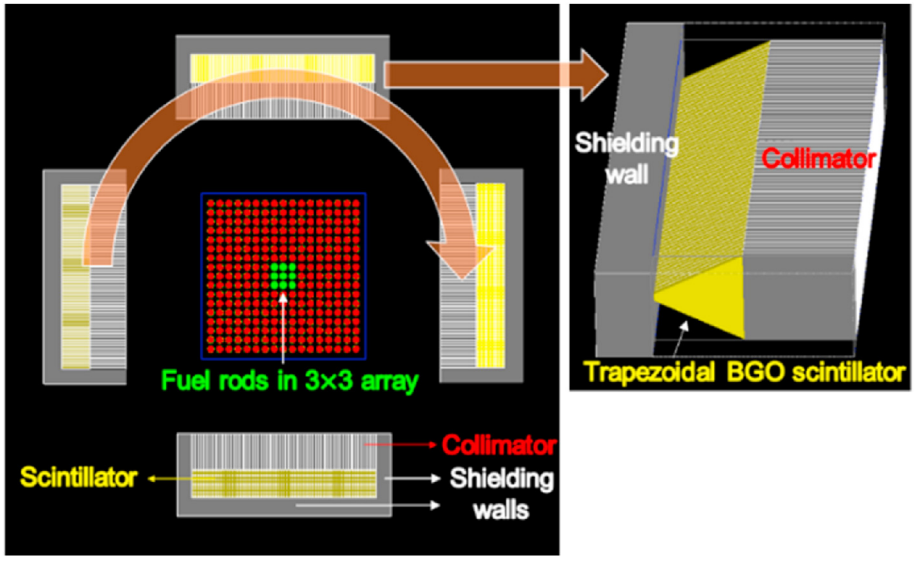

Fig. 1. MC simulation conditions for acquisition of tomographic images of various patterns of fuel rods within 3 × 3 array emitting 662 keV gamma-rays, using rotational four 64-channel detectors.

developed by Microsoft Research in 2015. ResNet, applied with a residual learning method that provides a shortcut for adding of input values to the output value, was proposed in order to overcome the limitation, discovered by Microsoft's researchers, that deepening of the hierarchical structure in the deep learning model does not necessarily improve performance [18]. The hierarchical structure of the previously developed CNN model focused on finding the optimal function H(x) that can convert the input value x to the target value y, and conducted learning in the direction of minimizing 'H(x)-y'. ResNet, by contrast, focuses on minimizing 'H(x)-x' based on the fact that y can be represented as x. In this manner, residual learning can proceed by minimizing 'F(x) = H(x)-x', the residual of the input value and the output value (H(x)), and the output value can be defined as 'H(x) = F(x) + x'. Further, ResNet uses a skip connection method whereby the output of one specific layer skips several layers and is added to the input of the next layer for more efficient operation that does not entail any increase in the number of parameters. This contrasts with the VGG models, by which only the output value of a specific layer is used as the input value in the next layer. Based on these structural characteristics, the deeper hierarchy of ResNet affords better performance.

All three models (VGG16, GoogLeNet, ResNet) consist of a fairly deep and complex structure for high-performance image recognition or classification suitable to the complex pattern and color map of the CIFAR-10 dataset consisting of 60000 color images in 10 classes with 50000 training images and 10000 test images. However, the models' training procedures for the CIFAR-10 dataset would incur huge computational costs and take much time. In the present study, the pattern and color map of the tomographic image of the 3 × 3 fuel assembly were relatively quite simple, and correspondingly, the structures of the VGG16, GoogLeNet, and ResNet models were simplified to reduce the numbers of parameters required for model training while maintaining the characteristics of each model. The structure of VGG16 was converted from five unit modules to three modules, and then the number of parameters required for training was reduced by 85% from 138,356,392 to 21,810,345. Accordingly, the training time was reduced by about a factor of 40. Meanwhile, the structure of GoogLeNet was converted from nine unit modules to two modules, and then the number of parameters required for training was reduced by 98% from 10,324,683 to 208,817. Accordingly, the training time was reduced by about 55 times. Finally, the structure of ResNet was converted from four unit modules to two modules, with one shortcut in the residual learning process, and then the number of parameters required for training was reduced by 37% from 23,546,761 to 14,871,665. Accordingly, the training time was reduced by about 17 times.

2.3. AI-based fuel-rod pattern analysis of tomographic images

The VGG16, GoogLeNet, and ResNet models were trained for analysis of fuel-rod patterns on low-quality tomographic images of a 3 × 3 fuel assembly. The fuel-rod patterns were assessed by analyzing averaged image intensities in nine regions of interest (ROIs) where the nuclear fuel rods were located in the 3 × 3 array (as illustrated in Fig. 2) and by predicting fuel-rod presence in each ROI. As illustrated in Fig. 3, the three AI models were trained for ten different conditions using an image dataset consisting of low-quality images reconstructed by the FBP algorithm (as FBP images) and ground truth (GT) images showing the actual pattern of fuel rods in the assembly. The five conditions for training of the three AI models were the five different FBP-GT image dataset sizes, which ranged from 100 to 500 image sets arbitrarily extracted from the total of 511 image sets. Under these five conditions, tomographic images were acquired by scanning the 3 × 3 fuel assembly for 450 s with the SPECT system. Five additional conditions were the five different FBP image qualities obtained with five different SPECT system scan times ranging from 450 to 4500 s. As the scan time was shortened, the noise level of the FBP images was increased and the fuel-rod patterns on those images became distorted. Under these five scan time conditions, the 500 randomly extracted FBP-GT image sets were used for model training. For optimization of model training, the Adam algorithm was used, and the learning rate was set to 0.0001. A total of 50 epochs were set for each of the three AI models. Using the AI model trained under each condition, the fuel-rod pattern recognition accuracy was evaluated for the rest of the 11 FBP images, except for those used in training, ten times.

3. Results and discussion

3.1. AI model performance according to data size

In this study, we used the 3 × 3 fuel-rod array to verify the feasibility of fuel-rod pattern estimation with an AI model by analyzing the averaged image intensities of the nine ROIs. Compared with the full size of the fuel assembly, a 17 × 17 array of fuel rods, the 3 × 3 array was small enough to generate tomographic images for all of the 511 (2^9-1) patterns with the MC simulation, which fact enabled us, moreover, to train the AI model with most of the images. However, for the full-size fuel assembly, considerable computational cost is incurred in generating tomographic images for all 9.95e+86 (2^{289}-1) patterns and in training the AI models. Therefore, we evaluated how the pattern estimation accuracy of the three AI models changed according to model training with different image datasets for percentages of the total 511 patterns ranging from about 20 to 98%. The reason for using training images of the lowest quality as obtained for 450 s scan time was to examine the dramatic changes in the pattern estimation accuracy of the AI models. Table 1 shows the evaluation results for the estimation accuracy of fuel-rod presence in each ROI on the tomographic image for the three AI models trained with the five different image set sizes. For the 500 image set, representing 98% of the total number of fuel-rod patterns, all of the AI models successfully estimated the presence or absence of fuel rods in the nine ROIs with 100% accuracy. It was difficult to compare the results in relation to the unique characteristics of the three AI models, because their parameter reduction rates are different. However, even though the number of parameters used in the training process for ResNet was about 32% less than that for VGG16, relatively better results were derived in terms of AI model performance. Therefore, the ResNet model can be advantageous to employ for future verification studies with fuel assemblies larger than 3 × 3. And because of the difficulty of generating a training image dataset for a larger size of fuel assembly by MC simulation, in a future study, we will apply a data-augmentation technique based on the structural symmetry of the assembly.

3.2. AI model performance according to image quality

Through this study, our ultimate goal is to develop a technique of fast verification by acquisition of a tomographic image of a spent-fuel assembly. Generally, the faster the scan speed of the SPECT system is, the worse the image quality will be. Therefore, it was necessary for us to evaluate the three AI models in order to determine if they can accurately verify fuel-rod patterns in tomographic images when image quality is degraded to certain extents. Fig. 4 shows the five images reconstructed by the FBP algorithm using multiple projection data obtained with a rotating SPECT system for 450, 1125, 2250, 3375, and 4500 s for the fuel-rod

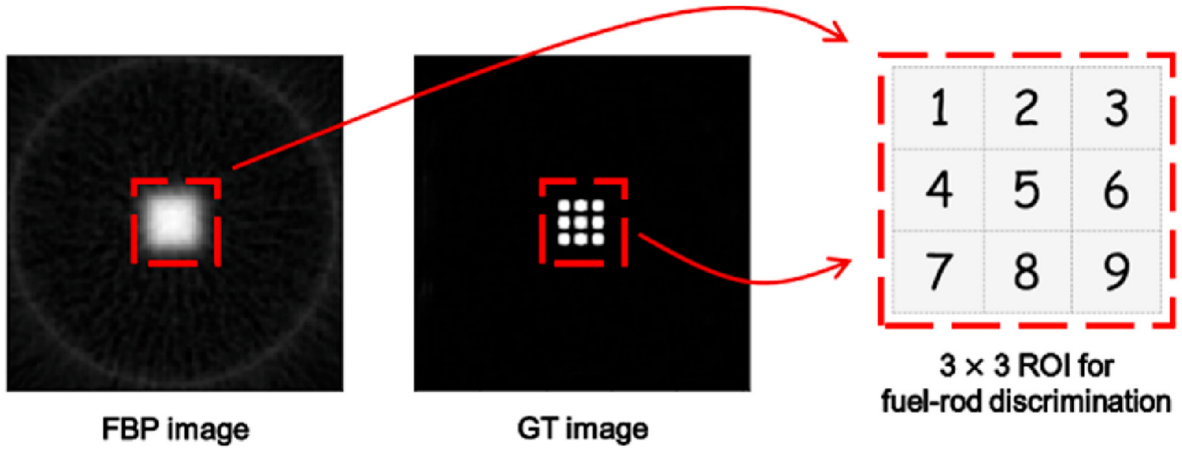

Fig. 2. Tomographic image intensity analysis within 3 × 3 region of interest (ROI) for fuel-rod discrimination.

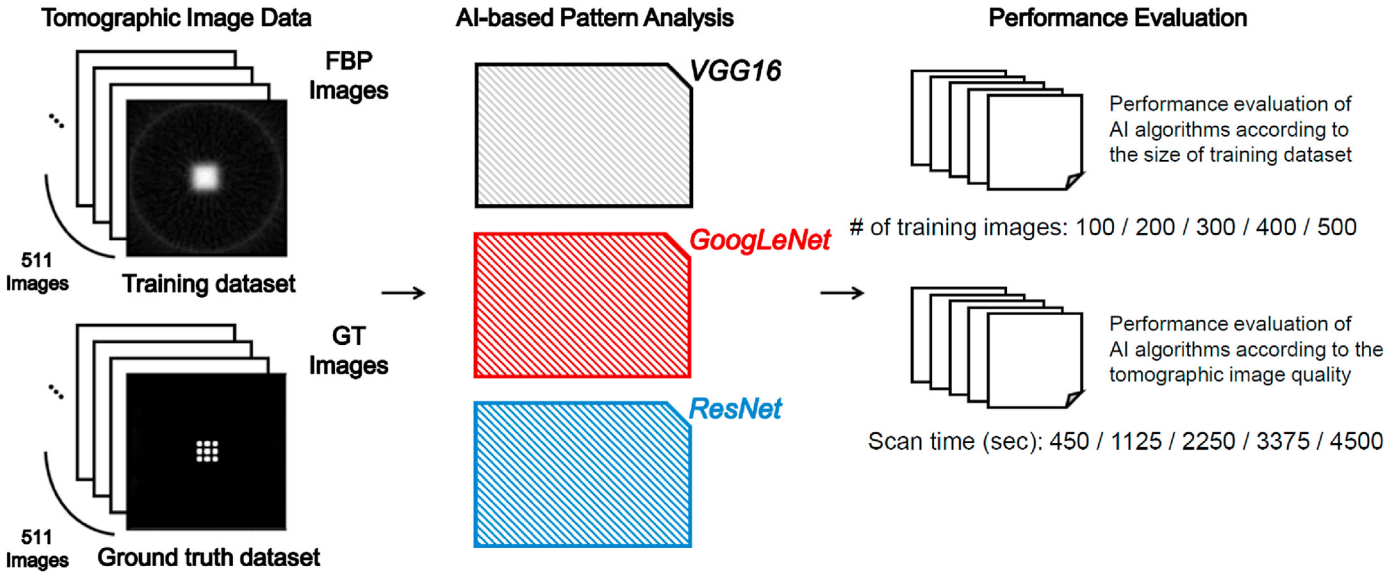

Fig. 3. Performance evaluation of three artificial intelligence models (VGG16, GoogLeNet, ResNet) trained with five different tomographic image set sizes and five different tomographic image qualities for fuel-rod pattern analysis.

Table 1
Performance evaluation of VGG16, GoogLeNet, and ResNet models trained with five different tomographic image set sizes (100, 200, 300, 400, 500 images).

		Accuracy of fuel rod discrimination (%)									Ave.
Image # for AI training	AI Model	ROI 1	ROI 2	ROI 3	ROI 4	ROI 5	ROI 6	ROI 7	ROI 8	ROI 9	
100	VGG16	90.8	86.1	69.1	99.3	70.3	95.9	98.8	92.7	83.2	87.3
	GoogLeNet	46.7	48.2	43.3	53.3	43.6	43.3	44.5	75.9	43.3	49.1
	ResNet	100	100	100	100	100	100	100	100	100	100
200	VGG16	96.1	81.7	84.9	99.0	72.3	72.7	97.4	96.1	83.3	87.0
	GoogLeNet	89.4	38.6	37.9	52.7	81.4	72.0	41.2	76.8	67.5	61.9
	ResNet	100	100	100	100	100	100	100	100	100	100
300	VGG16	98.6	100	87.7	100	96.7	100	99.5	91.5	99.5	97.1
	GoogLeNet	86.7	57.8	83.9	45.0	86.3	73.5	59.7	82.9	91.9	75.3
	ResNet	100	100	100	100	100	100	100	100	100	100
400	VGG16	100	100	95.5	98.2	100	100	100	100	96.4	98.9
	GoogLeNet	100	93.7	74.8	83.8	90.1	90.1	100	90.1	89.2	90.2
	ResNet	100	100	100	100	100	100	100	100	100	100
500	VGG16	100	100	100	100	100	100	100	100	100	100
	GoogLeNet	100	100	100	100	100	100	100	100	100	100
	ResNet	100	100	100	100	100	100	100	100	100	100

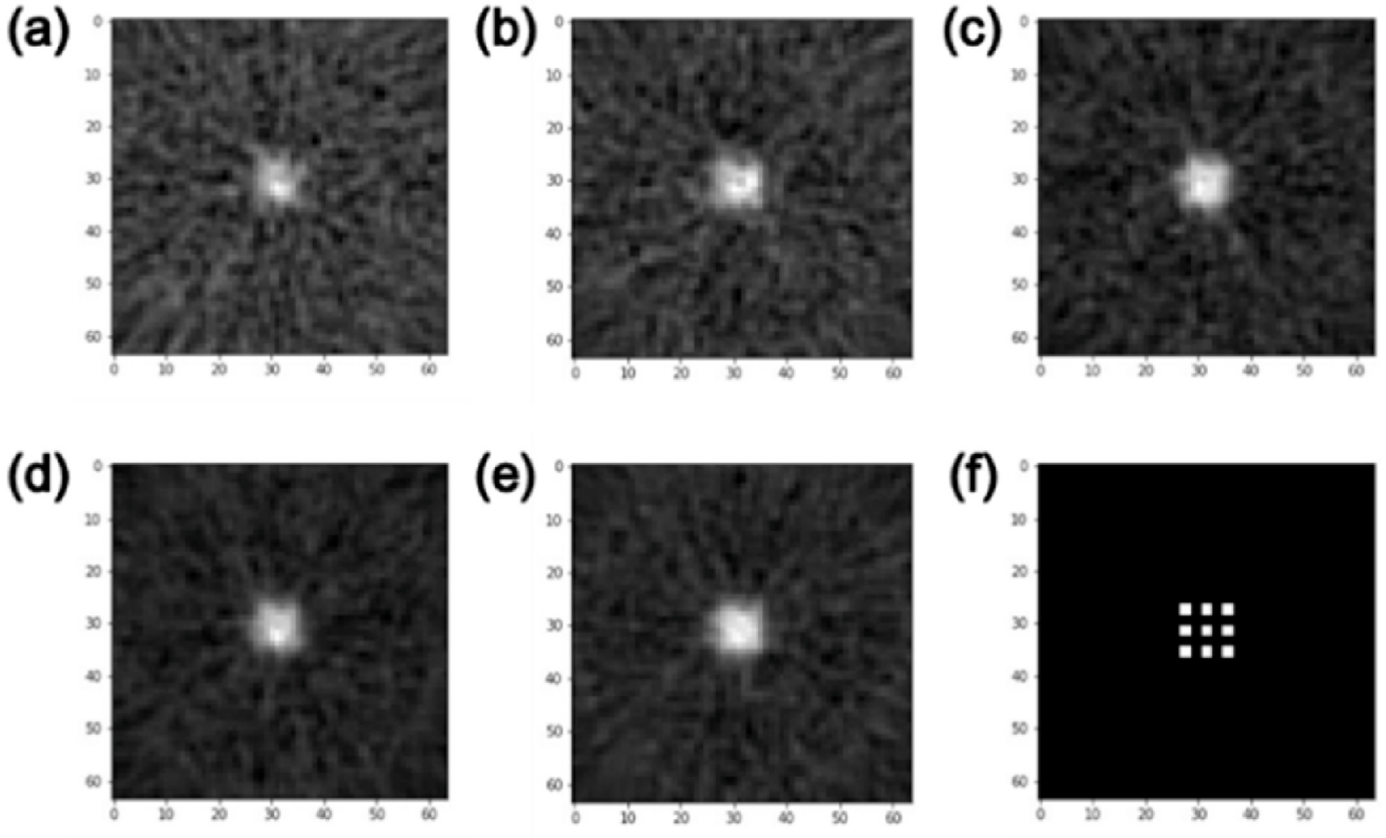

Fig. 4. Five different tomographic image qualities obtained in scan times of (a) 450, (b) 1125, (c) 2250, (d) 3375, (e) 4500 s for fuel-rod pattern illustrated in (f) GT image.

Table 2
Performance evaluation of VGG16, GoogLeNet, and ResNet models trained with tomographic images of 500 fuel-rod patterns obtained within five different scan times (450, 1125, 2250, 3375, 4500 s).

		Accuracy of fuel rod discrimination (%)									Ave.
Scan time (sec.)	AI Model	ROI 1	ROI 2	ROI 3	ROI 4	ROI 5	ROI 6	ROI 7	ROI 8	ROI 9	
450	**VGG16**	100	100	100	100	100	100	100	100	100	100
	GoogLeNet	100	100	100	100	100	100	100	100	100	100
	ResNet	100	100	100	100	100	100	100	100	100	100
1125	**VGG16**	100	100	100	100	100	100	100	100	100	100
	GoogLeNet	100	100	100	100	100	100	100	100	100	100
	ResNet	100	100	100	100	100	100	100	100	100	100
2250	**VGG16**	100	100	100	100	100	100	100	100	100	100
	GoogLeNet	100	100	100	100	90.9	100	100	100	100	98.9
	ResNet	100	100	100	100	100	100	100	100	100	100
3375	**VGG16**	100	100	100	100	100	100	100	100	100	100
	GoogLeNet	100	100	100	100	100	100	100	100	100	100
	ResNet	100	100	100	100	100	100	100	100	100	100
4500	**VGG16**	100	100	100	100	100	100	100	100	100	100
	GoogLeNet	100	100	100	100	100	100	100	90.9	100	98.9
	ResNet	100	100	100	100	100	100	100	100	100	100

pattern illustrated in Fig. 4(f). Table 2 shows the evaluation results of the estimation accuracy of fuel-rod presence in each ROI on tomographic images for the three AI models trained with five different image dataset qualities, each dataset consisting of 500 tomographic images. The VGG16 and ResNet models successfully estimated the presence or absence of fuel rods in the nine ROIs with 100% accuracy in all cases, while the GoogLeNet model was evaluated at 98.9% prediction accuracy for both scan times of 2250 and 4500 s. This result might have been due to the fact that the total number of parameters used for training the GoogLeNet model in this study was too small, and that therefore, its performance became unstable. Nevertheless, the overall results demonstrated the applicability of an AI model, even for image quality so low as to render image recognition by people difficult. In other words, an AI model can be effectively employed to accurately verify fuel-rod patterns using tomographic images obtained with a high-speed scan. Based on this determination, we will employ this AI-based pattern analysis technique for tomographic images of larger assemblies that may have many image artifacts due to the higher scattering and attenuation probabilities of gamma-rays emitted

from assembly interiors. For this, further studies are necessary not only to optimally design an AI model but also to evaluate its performance for various patterns of image artifacts on low-quality tomographic images.

4. Conclusion

In this paper, we have proposed an artificial intelligence (AI)-based tomographic image analysis technique that can discriminate fuel-rod patterns, even with low-quality images acquired with a high-speed scan. With Monte Carlo (MC) simulation as an alternative to experimentation, tomographic images for various fuel-rod patterns in a 3 × 3 fuel assembly were obtained, and the pattern-discrimination performances of the VGG16, GoogLeNet, and ResNet AI models were evaluated. We demonstrated that these models can effectively facilitate accurate and fast verification of fuel assemblies.

Through our previous studies [10,11], we confirmed that the large-sized scintillator detector than the small-sized semiconductor detector of PGET showed considerable higher sensitivity even for the gamma-rays emitted by the most internal fuel rod in the full-sized (e.g. 17 × 17) assembly stored in water storage, furthermore, tomographic image quality can be considerably improved with a deep learning-based de-noising technique. Further, we will develop an advanced attenuation correction method, accordingly, we expect that the in-house SPECT system, named Yonsei single-photon emission computed tomography (YSECT), is able to obtain a high-quality tomographic image of the full-sized fuel assembly in water in the future. Then, the AI-based tomographic image analysis technique proposed in this study can be effectively employed for the purpose of shortening pin-by-pin verification time. We will evaluate our image analysis technique's availability for additional and various conditions such as the number of fuel rods, the hierarchical depth of the AI structure, the number of hyper-parameters, the presence or absence of artifacts on tomographic images, and the uniformity of fuel-rod image intensity on tomographic images.

Declaration of competing interest

The authors declare that they have no known competing financial interests or personal relationships that could have appeared to influence the work reported in this paper.

Acknowledgments

This research was supported by the Basic Science Research Program through the National Research Foundation of Korea (NRF) funded by the Ministry of Education (NRF-2021R1I1A1A01059875), the Nuclear Safety Research Program through the Korea Foundation Of Nuclear Safety (KoFONS) using financial resources granted by the Nuclear Safety and Security Commission (NSSC) of the Republic of Korea (No. 2101073), the Korea Institute of Energy Technology Evaluation and Planning (KETEP), and the Ministry of Trade, Industry & Energy (MOTIE) of the Republic of Korea (No. G032579811).

References

[1] D. Sweeney, Additional Detection Techniques under Development, Spent Nuclear Fuel Safeguards, Texas A&M University, Nuclear Security and Safeguards Education Portal, 2017, p. 35, chap. “Safeguards”.
[2] I.A.E.A. International, Safeguards in the Design of Facilities for Long Term Spent Fuel Management, IAEA NUCLEAR ENERGY SERIES, 2018, pp. 10–42. NF-T-3.1.
[3] M. Zendel, IAEA safeguards equipment, Int. J. Nucl. Sci. Technol. 4 (1) (2008) 72–80.
[4] T. Honkamaa, A. Turunen, F. Levai, M. Larsson, R. Berndt, A. LeBrun, Prototype Tomographic Partial Defect Tester, 2006. No. IAEA-CN–148).
[5] T. Honkamaa, A. Turunen, F. Levai, M. Larsson, R. Berndt, A. LeBrun, Prototype tomographic partial defect tester: project status update, in: Proceedings of an International Safeguards Symposium on Addressing Verification Challenges, Posters, 2007.
[6] T. Honkamaa, F. Levai, A. Turunen, R. Berndt, S. Vaccaro, P. Schwalbach, A Prototype for passive gamma emission tomography, in: IAEA Symposium on International Safeguards: Linking Strategy, Implementation and People, Vienna, 2014.
[7] S. Holcombe, S.J. Svard, L. Hallstadius, A Novel gamma emission tomography instrument for enhanced fuel characterization capabilities within the OECD Halden Reactor Project, Ann. Nucl. Energy 85 (2015) 837–845.
[8] E.L. Smith, S. Jacobsson, V. Mozin, P. Jansson, E. Miller, T. Honkamaa, et al., Viability Study of Gamma Emission Tomography for Spent Fuel Verification: JNT 1955 Phase I Technical Report, 2016.
[9] E.A. Miller, L.E. Smith, R.S. Wittman, L.W. Campbell, N. Deshmukh, M.A. Zalavadia, et al., Hybrid Gama Emission Tomography (HGET): FY16 Annual Report NO. PNNL-26213, Pacific Northwest National Lab.(PNNL), 2017. Richland, WA United States.
[10] H.J. Choi, I.S. Kang, K.B. Kim, Y.H. Chung, C.H. Min, Optimization of single-photon emission computed tomography system for fast verification of spent fuel assembly: a Monte Carlo study, J. Instrum. 14 (2019) T07002, 07.
[11] S.H. Choi, H.J. Choi, C.H. Min, Y.H. Chung, J.J. Ahn, Development of de-noised image reconstruction technique using Convolutional AutoEncoder for fast monitoring of fuel assemblies, Nucl. Eng. Technol. 53 (3) (2021) 888–893.
[12] M.D. Zeiler, R. Fergus, Visualizing and Understanding Convolutional Networks, Computer Vision-ECCV, 2014, pp. 818–833.
[13] A. Krizhevsky, I. Sutskever, G.E. Hinton, Imagenet classification with deep convolutional neural networks, Adv. Neural Inf. Process. Syst. (2012) 1097–1105.
[14] K. Simonyan, A. Zisserman, Very deep convolutional networks for large-scale image recognition, 2014, p. 1556, arXiv preprint arXiv:1409.
[15] C. Szegedy, W. Liu, Y. Jia, P. Sermanet, S. Reed, D. Anguelov, et al., Going deeper with convolutions, IEEE Comput. Soc. Conf. Comput. Vis. Pattern Recogn. (2015) 1–9.
[16] L. Wang, C.Y. Lee, Z. Tu, S. Lazebnik, Training Deeper Convolutional Networks with Deep Supervision, 2015, 02496 arXiv preprint arXiv:1505.
[17] C.Y. Lee, S. Xie, P. Gallagher, Z. Zhang, Z. Tu, Deeply-supervised nets, Int. Conf. Artif. Intell. Stat. (2015) 562–570.
[18] S. Targ, D. Almeida, K. Lyman, Resnet in Resnet: Generalizing Residual Architectures, 2016, 08029 arXiv preprint arXiv:1603.